INTERNATIONAL JOURNAL OF APPLIED SCIENCE ENGINEERING AND MANAGEMENT

www.ijasem.org

Utilising modified direct torque control and adaptive control theory for regenerative braking in electric vehicles

[1]S. Sarvani, [2]P. Tejasree, [3]P. Pavani, [4]CH. Krishna Chaitanya, [5]D. Dhanush

[1]Assistant Professor, Dept. of EEE, NSRIT, Visakhapatnam, AP

[2,3,4,5,6,7] B. Tech Students, Dept. of EEE, NSRIT, Visakhapatnam, AP

NSRIT-Nadimpalli Satyanarayana Raju Institute of Technology

ABSTRACT: - This paper provides a revolutionary electric vehicle regenerative braking method. The suggested. The short-range battery discharge issue is resolved by the procedure. In order to recuperate electrical energy from electric vehicles, the direct torque control switching algorithm has been updated. Without the use of an extra power converter or other electrical energy storage devices, operated by brushless direct-current motor. Due to the unique arrangement of voltage vectors during the regenerative braking process, the inverter is subjected to switching patterns that are distinct from those used during normal operation. It is believed that the new switching pattern transforms mechanical energy into electrical energy. The proposed solution uses the battery's state of charge as a performance indicator. A model reference adaptive system is simultaneously created to adjust the system's parameters. Several simulations are run to verify the efficiency and performance of the suggested methods. The outcomes demonstrate the excellent competence of the devised techniques.

1. Introduction

The need for employing renewable energies is becoming clearer at this time due to worries about global warming, the price of fossil fuels, and the unpredictability of oil supplies [1-3]. As a result, the government has altered its regulations to encourage automakers to set aside money for EV research [1,4]. There are also certain disadvantages of EVs that can be highlighted as compared to conventional cars, including the battery pack, charging mechanism, and a limited range due to the battery's charging capacity [4-5]. As a result, automakers have worked to enhance their products' standard quality and fuel efficiency in response to public requests and government directives [5].

High-tech components like sensors, additional storage, and inverter circuits can be used to improve the efficiency of EVs. However, these technologies could make EVs more difficult to use while also raising the overall cost of making EVs [6]. Therefore, by altering the regenerative braking system, researchers are attempting to solve this issue. Three important parts of EVs are the battery pack, the motor drive system, and the converter controller [4]. Power transmission mechanisms heavily rely on motor drive system technology [3]. Switched reluctance machines (SRM), induction motors (IM), and brushless direct-current (BLDC) motors are the common electric motors utilised in EVs [3]. The BLDC motors are the most popular

type among them. The majority of Brushless DC motor applications can be divided into four categories: servo drives, appliances, medical equipment, and a wide range of power systems [7]. Its widespread use can be attributed to its high effectiveness, optimum torque-speed characteristic, dependability, stability, lower noise, and straightforward control structure [7-8]. The primary flaw in BLDC motors, however, is the torque ripple, which leads to cogging torque [9].

Another important factor in this type of motor's ability to maintain the windings in the proper rotational direction is awareness of the rotor's precise position [10]. Due to their low cost, the Hall sensors are used to detect these positions, especially in areas where phase currents need to be switched on and off. When the magnetic poles of the rotor pass in front of the proximity sensors, they detect the rotor's pole sign [11]. The precise order of commutation is determined by evaluating the received signals. The combinational logic can be understood to decode the signals. There are six voltage vectors as outputs. Therefore, the phases are subjected to the firing commands in order to conduct them to 120 electrical degrees.

There are several methods that have been suggested to control BLDC motors, including direct torque control (DTC), dc link current control, hysteresis current control, and pulse width modulator control [12]. DTC is the most dependable of these methods. Based on the instructions received from the controller, a three-phase switching circuit is employed to operate the motors [3]. DTC switching patterns can be changed in a variety of ways with various objectives. Numerous publications have previously been released to enhance EVs' regenerative braking techniques in numerous procedures with various motors [13–16]. The ability to

reuse brake energy can significantly improve energy efficiency [15], which is a key distinction between EVs and conventional automobiles. By applying regenerative braking, the motor generates power as the energy is reversed into the battery and used to slow down the vehicle [10–11]. [17] introduces a brand-new switching pattern based on the rotor location at various running speeds. even if in the suggested approach. In order to address stator overheating, a closed-loop temperature controller is needed to maintain the high level of braking torque. The journey of the car can be extended by recovering potential and kinetic energy while declaration or stopping. Some of the suggested ways simply make the system more complex by including extra hardware like sensors, extra storage, and new inverter circuits [14]. The proposed solution makes just minor structural changes to the switching pattern to recover the lost kinetic energy. Based on how they affect torque and flux, voltage vectors are arranged in descending order. The controller serves as the brains of the system that drives and brakes motors using regenerative energy. Proportional-integral (PI) controllers are a widely common type of control system because of their straightforward design and quick torque and speed responses. However, this controller's performance suffers in the face of speed variations, parameter fluctuations, and load effects [16,18]. Under mode changeover in DTC, one of the situations where PI controller is inefficient and needs to be replaced with alternative controllers. An effective algorithm is used in [19] to solve this issue. In this study, a model reference adaptive system (MRAS) is used to follow the reference speed signal and automatically tune the controller parameters. The effectiveness of the suggested approach is

https://doi.org/10.5281/zenodo.14090580

assessed in the section on simulation results, where the new regenerative braking technique is used in parallel with the adaptive controller to improve the battery's state of charge (SOC) during a 0.9-second simulation by 0.6% in comparison to the traditional switching pattern and PI controller. This energy conservation can increase the driving range of EVs. In terms of response time and steady-state tracking error, the suggested controller outperforms the traditional PI controller.

This essay is set up as follows. By estimating the resistance forces on the vehicle, Section 2 describes the EV's dynamic behaviour. The typical DTC for BLDC motor is analysed in Section 3, which also demonstrates how the speed vectors should be chosen to satisfy the needs of changing the flux linkage and electromagnetic torque. In Section 4, a brand-new DTC algorithm is suggested in order to enhance battery state of charge. This technique involves altering the switching order without the use of an additional power converter or other electrical energy storage systems. A more effective MRAS than the previous controller is introduced in Section 5. The results of the simulations are described in Section 6. For this part, a driving cycle alike to the urban driving cycle ECE and genuine parameters of an EV are picked. Section 7 brings the paper's conclusion to a close.

2. Dynamic model of electric vehicle

The forces exerted on the vehicle can be used to analyse its motion and acceleration. The following formulas [4] can be used to represent the resistance forces exerted on the EV in the motoring mode:
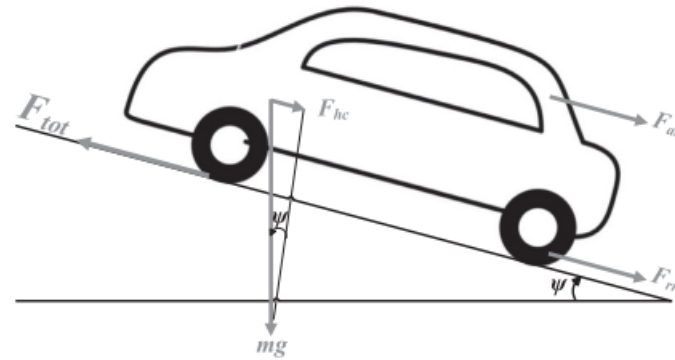
$$F_{tot} = F_{rr} + F_{hc} + F_{ad} + F_{la}$$

Fig. 1. The forces acting on a vehicle moving along the slope.

$$F_{rr} = M.g.f \text{ is the rolling resistance} \tag{2}$$

$$F_{hc} = M.g.\sin\psi \text{ is the hill climbing force} \tag{3}$$

$$F_{ad} = \frac{1}{2}\rho.C_d.A.v^2 \text{ is the aerodynamic drag} \tag{4}$$

$$F_{la} = M.\frac{dv}{dt} \text{ is the acceleration force} \tag{5}$$

where g is the acceleration caused by gravity, f is the rolling resistance coefficient, is the air density, Cd is the aerodynamic drag coefficient, v is the vehicle's speed, A is its frontal area, M is its total mass, and is the slope angle.

The formula for calculating the total torque load is (6) in:

$$T_L = F_{tot} * R_w \tag{6}$$

where Rw denotes the tire's circumference.

By generating tractive force, an electric motor is responsible for overcoming overload force [19]. The most popular motors used in EVs to improve performance are BLDC motors. Fig. 2 depicts the BLDC drive system's general switching circuit.

Equation (7) is used to illustrate the BLDC equivalent dynamic model.

https://doi.org/10.5281/zenodo.14090580

$$\begin{bmatrix} V_{an} \\ V_{bn} \\ V_{cn} \end{bmatrix} = \begin{bmatrix} R & 0 & 0 \\ 0 & R & 0 \\ 0 & 0 & R \end{bmatrix} \begin{bmatrix} i_a \\ i_b \\ i_c \end{bmatrix} + \begin{bmatrix} L & 0 & 0 \\ 0 & L & 0 \\ 0 & 0 & L \end{bmatrix} \frac{d}{dt} \begin{bmatrix} i_a \\ i_b \\ i_c \end{bmatrix} + \begin{bmatrix} e_a \\ e_b \\ e_c \end{bmatrix}$$

$$L = L_s - L_m$$

where Van, Vbn, and Vcn are the phase voltages, ia, ib, and ic are the phase currents, R are the phase resistances, L are the equivalent inductance in each stator winding, Ls are the inductance of each phase, Lm are the mutual inductance between phases, and ea, eb, and ec are the back-EMFs of each phase.

Figure 3 shows the ideal current and back-EMF signals for one of the phases.

3. Direct torque control of BLDC

BLDC motors are managed using the direct torque control (DTC) approach. which induction motors were used to implement [20]. It is widely used in industrial applications due to its great performance in regulating variable speed drives. This technique concurrently and independently regulates the electromagnetic torque and the flux linkage. Additionally, DTC has a strong dynamic performance, quick torque response, simplicity, and resistance to uncertain parameters. However, it has changing and rippled torque.
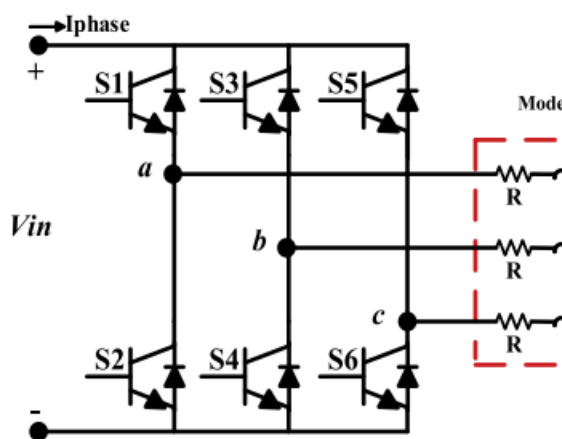

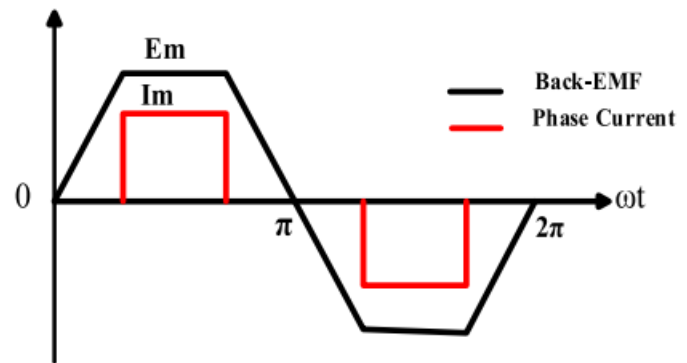Fig. 2. A general schematic of BLDC drive.

Fig. 3. The ideal waveform of back-EMF and current.

occurrences [11]. The DTC method heavily relies on electromagnetic torque. The electromagnetic torque in a stationary () reference frame is described by equation (9) [20]:

$$T_{em} = \frac{3}{2}\frac{P}{2}\left[\frac{d\phi_{r\alpha}}{d\theta_e}i_{s\alpha} + \frac{d\phi_{r\beta}}{d\theta_e}i_{s\beta}\right] = \frac{3}{2}\frac{P}{2}\left[\frac{e_\beta}{\omega_e}i_{s\alpha} + \frac{e_\alpha}{\omega_e}i_{s\beta}\right]$$

where e is the electrical rotor position, is, is are stator currents, e, e are back-EMF, e is the electrical rotor position, and r, r, are electromagnetic torques in the reference frame.

DTC selects the appropriate voltage vector from a set of six or eight space vectors based on a certain set of instructions. The potential space vectors and patterns that DTC may employ to select the appropriate voltage. Based on the outputs from the hysteresis controller, commands are selected. The inputs to the hysteresis controller are the differences between the estimated and real values of torque and flux. For flux linkage, this inaccuracy is known as the FST, and for electromagnetic torque, it is known as the TST. The need for an increase or decrease in flux, respectively. Additionally, the unmodified situations are displayed using the "F" expression [21].

https://doi.org/10.5281/zenodo.14090580

The DTC block diagram is shown in Fig. 4, and it includes the switching table, flux and torque estimators, and speed and hysteresis controllers. The PI speed controller generates the reference electromagnetic signal during DTC switching system operation using the difference between the reference and measured speeds. The hysteresis controller receives the deviations between the desired and actual extents of the flux linkage and electromagnetic torque in order to provide the instruction based on the switching pattern table for the inverter [20].

4. The modified regenerative braking DTC

In the BLDC motor's driving mode, the stator flux vector advances in front of the rotor flux. Rotating the rotor and stator flows in the opposing directions is necessary to generate inverse torque. In order to ensure that the stator flux follows the rotor flux and supplies power to the battery, the appropriate voltage vector must be provided to the inverter. For the switching pattern, there is no state to provide inverse torque in standard DTC. Therefore, when a sharp drop in torque is necessary, the zeros vectors are used. As a result, reducing reversibility reduces motor speed and slows dynamic response [22]. When zeros are chosen as vectors, regeneration energy and abrupt braking result. Reversibility also reduces the motor speed and slows the dynamic response [22].
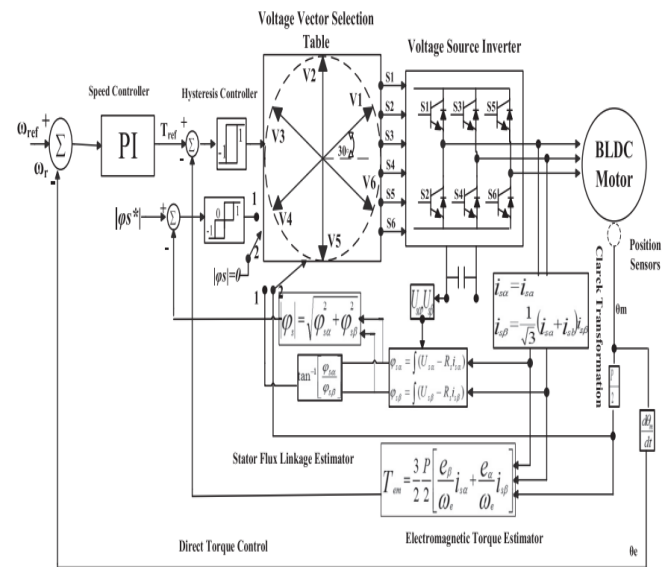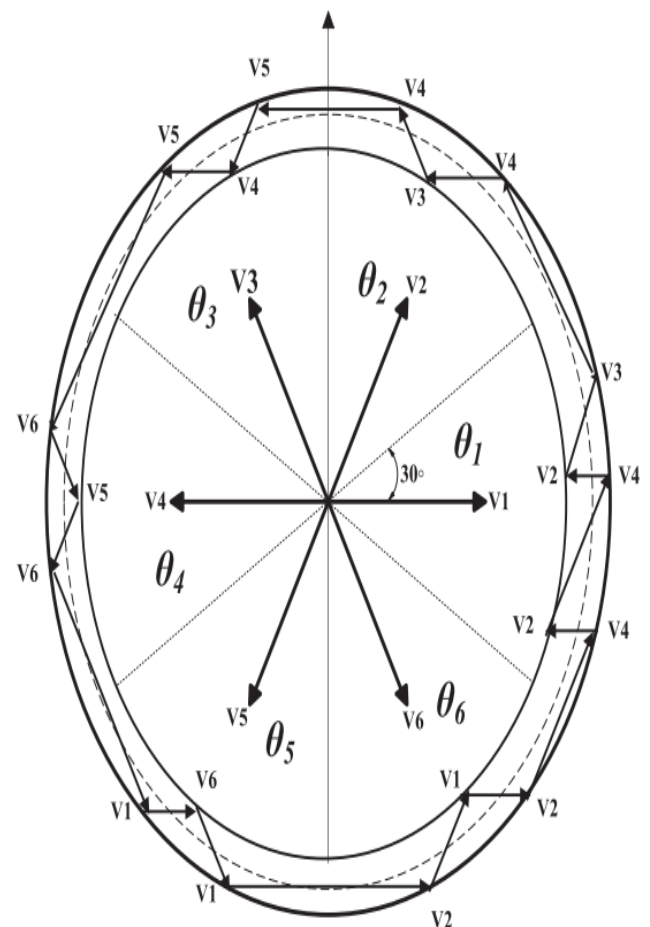

Fig. 4. General configuration of DTC with BLDC motor [12].

https://doi.org/10.5281/zenodo.14090580

Fig. 5. Voltage vectors and their role.

A few active voltage vectors are chosen for each sextet sector to regulate the magnitude of the flux-linkage. The exerted configurations are displayed in F.

In this study, the switching pattern was changed to enhance the widely used DTC technique and to recover energy from the braking system. Table 1 and Fig. 6 illustrate the vectors for different scenarios to raise or decrease the electromagnetic torque and flux and modify the results. Negative torque is provided to the motor using the updated switching sequence, which generates electrical energy that is passed through the reverse diodes to charge the storage devices. Fig. 7, the red line represents the system's regular operating mode (the motoring mode), and the blue line depicts the current flow during braking, which recharges the battery and raises the battery pack's state of charge (SOC). Phases A and B are powered in the motoring mode by S1 and S4. D1 and D4 are biased to return energy to the battery in the opposite direction during regenerative braking, which raises the battery pack's state of charge (SOC).

The two levels of the hysteresis controller in this method are subjected to the estimated flux inaccuracy. A three-level hysteresis controller has also been used to manage the torque in the following ways:

$$\text{Hystersis Output} = \begin{cases} 1 & \text{Increase the Torque} \\ 0 & \text{No change} \\ -1 & \text{Decrease the Torque} \end{cases}$$

Table. 1

Vectors selection based on increasing or decreasing flux and torque.

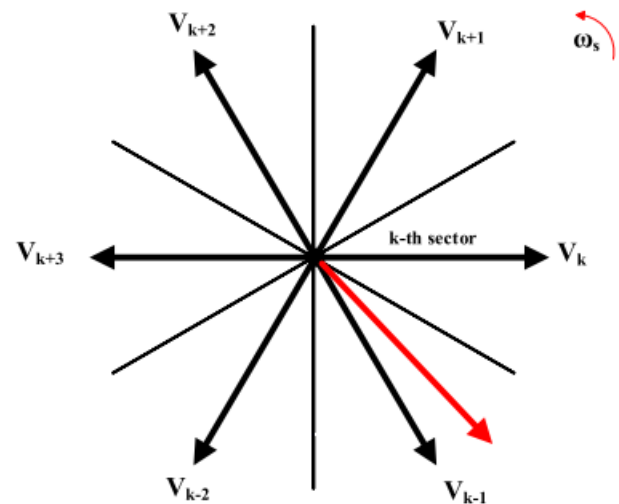| Voltage vector	Increase	Decrease
Flux	V_k, V_{k+1}, V_{k-1}	$V_{k+3}, V_{k+2}, V_{k-2}$
Torque	V_{k+2}, V_{k+1}	V_{k-2}, V_{k-2}

Fig. 6. The effect of selecting a voltage vector if the flux is in the k sector.
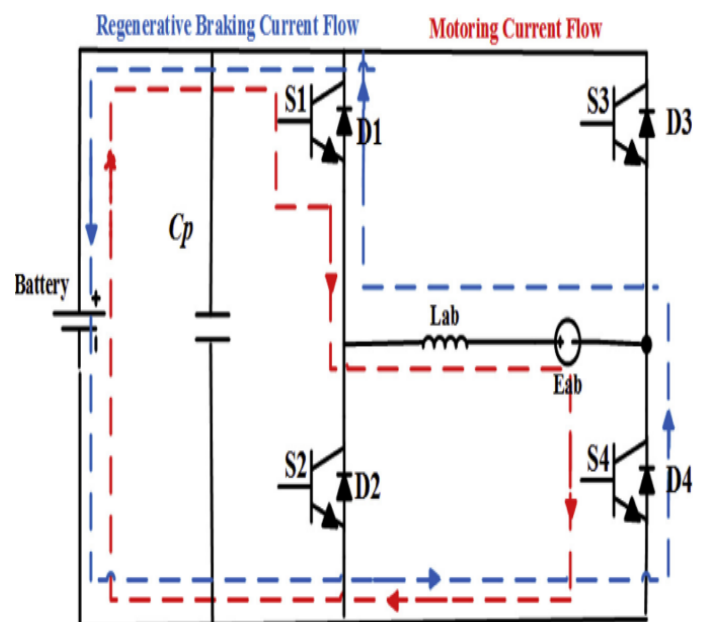

Fig. 7. The energy flow in different operation modes.

5. Model reference adaptive control

A MRAS controller is created to solve these issues and guarantee the zero-tracking

error because the conventional PI controller is not robust in the presence of parameter uncertainty and the disturbance signal [23–24]. The MRAS block diagram is displayed in Fig. 8 [3].

The model reference transfer function, or Gm(s), has the value kG s p p (. The proportional adaptive controller parameter kp controls the system in a way that the desired output signals follow the reference signals. Gp(s) is the system's corresponding transfer function. The control signal, u(t), is equivalent to kpuc(t).The adaptive controller constructs the required command using the error signal. The adaptive controller's primary goals are to provide system stability during uncertainty and disturbances.

Table. 2

The proposed switching table.

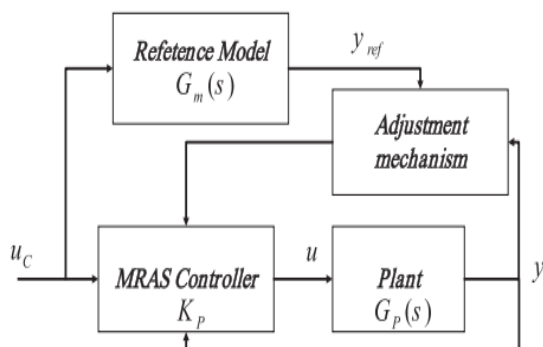| Tst	Fst	Sector					
		θ1	θ2	θ3	θ4	θ5	θ6
TI	FI	V2(001001)	V3(011000)	V4(010010)	V5(000110)	V6(100100)	V1(100001)
	FD	V3(011000)	V4(010010)	V5(000110)	V6(100100)	V1(100001)	V2(001001)
T	FI	V0(010101)	V7(101010)	V0(01010)	V7(101010)	V0(010101)	V7(101010)
	FD	V0(010101)	V7(101010)	V0(010101)	V7(101010)	V0(010101)	V7(101010)
TD	FI	V6(100100)	V1(100001)	V2(001001)	V3(011000)	V4(010010)	V5(000110)
	FD	V5(000110)	V6(100100)	V1(100001)	V2(001001)	V6(100100)	V4(010010)

Fig. 8. The general form of MRAS.

Zero tracking error and ensuring system stability in the face of uncertainty and disruptions are the main goals of the adaptive controller. The algorithm can be derived from control error, and the tuning process is known as the MIT rule:

$$e = y - y_m = L^{-1}(k_p G_p(s) U(s) - \bar{k}_p G_p(s) U(s))$$

The following is the cost function that needs to be minimised in order to change the adaption gain:

$$J(k_p) = \frac{1}{2} e^2(k_p) \tag{11}$$

The J's negative gradient can be used to scannable change the adaption parameter. This is how the tracking error is calculated:

$$
\begin{aligned}
e = y - y_m &= L^{-1}(G_p(s)k_p U(s) - G_p(s)\bar{k}_p U(s)) \\
&= L^{-1}(G_p(s)U(s)(k_p - \bar{k}_p)) \\
&= L^{-1}\left(\frac{G_p(s)U(s)\bar{k}_p(k_p - \bar{k}_p)}{\bar{k}_p}\right) = \frac{(k_p - \bar{k}_p)}{\bar{k}_p}L^{-1}(\bar{k}_p G_p(s)U(s)) \\
&= \frac{(k_p - \bar{k}_p)}{\bar{k}_p}L^{-1}(G_m(s)U(s)) = \frac{(k_p - \bar{k}_p)}{\bar{k}_p}L^{-1}(Y_m(s)) = \frac{(k_p - \bar{k}_p)}{\bar{k}_p}y_m
\end{aligned}
\tag{12}
$$

Also, from the Eq. (11):

$$J(k_p) = \frac{1}{2}e^2(k_p)$$

$$\frac{dk_p}{dt} = -\gamma \frac{\partial J}{\partial k_p} = -\gamma e \frac{\partial e}{\partial k_p} \tag{13}$$

Where $\frac{\partial e}{\partial k_p}$ is the system's sensitivity derivative, and is the gain from adaptation [25].

The MIT adaptation rule will be the following using Equations (12) and (13):

$$\frac{dk_p}{dt} = -\gamma e \frac{\partial e}{\partial k_p} = -\gamma e y_m \tag{14}$$

It should be noted that the MIT rule is very dependent on the signal's loudness. The system could become unstable for a signal with a big amplitude. The MIT rule is an excellent choice for enhancing system performance because the motor speed is a signal with a constrained range.

6. Simulation results and discussion

https://doi.org/10.5281/zenodo.14090580

MATLAB/Simulink simulations have been run to demonstrate the effectiveness of the suggested approach. Different scenarios have been taken into consideration to demonstrate the performance of the suggested technique. The motor's simulation-related properties are displayed in Table 3. Fig. 9 shows how the system's plant results from speed control and can be compared to a second-order system as shown in Eq. (15).

$$Gp = \frac{b_0}{s^2 + bs + a}$$

The following reference model is selected:

$$Gm = \frac{b_m}{s^2 + b's + a'}$$

Where $a = R/L + B/J, \; b = RB/LJ$

The reference model is typically constructed based on the desired output signals, such as settling time, rising time, and overshoot. It is important to keep in mind that there is no straightforward way for defining the reference model.

Table. 3

BLDC motor parameter and the parameters of PI controller.

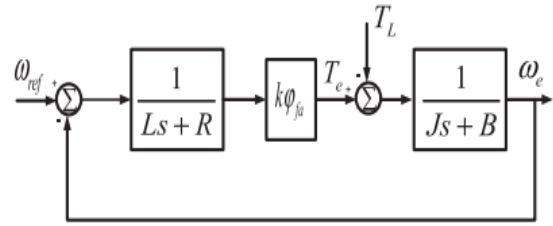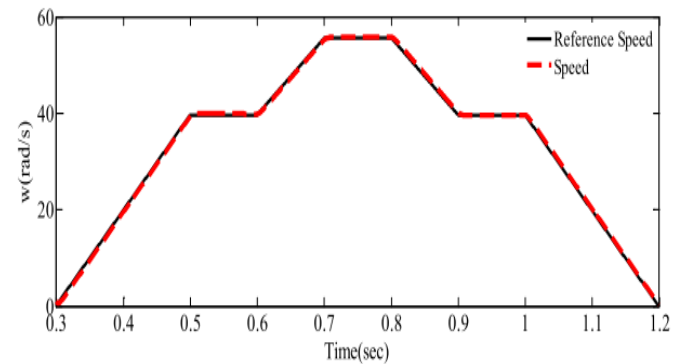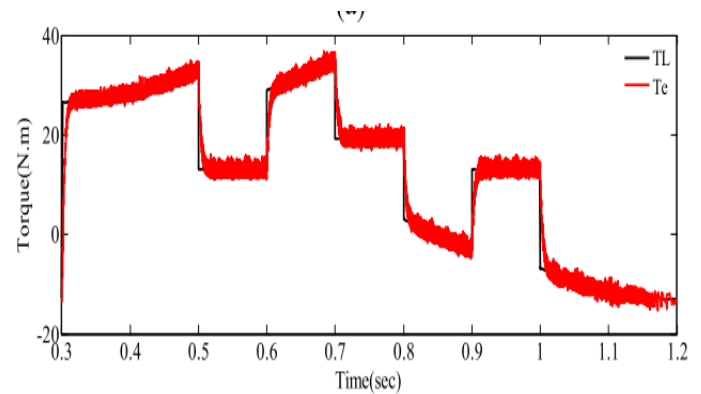| Parameter	Value	Unit
Number of poles	2	-
Phase resistance	0.2	[Ω]
Phase inductance	5	[mH]
DC link voltage	600	[v]
Moment of inertia	0.1	[kg m²]
Damping constant	0.002	[N.m.s]
Proportional gain, Kp	30	-
Integrator gain, Ki	200	-

Fig. 9. Block diagram of the closed-loop speed controller.

(a)

(b)

Fig. 10. (a) Speed tracking and demanded speed, (b) torque tracking of BLDC motor in common DTC.
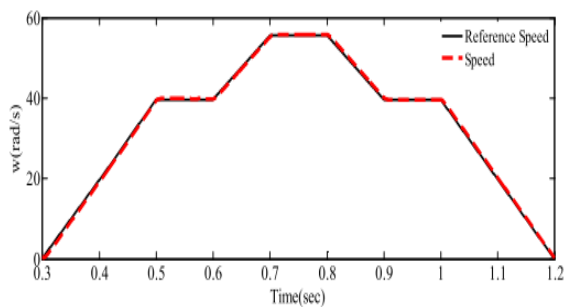
6.1. Conventional DTC

The motor has undergone a driving cycle that is comparable to the standard ECE driving cycle. Following temporary state, all figures are plotted out.
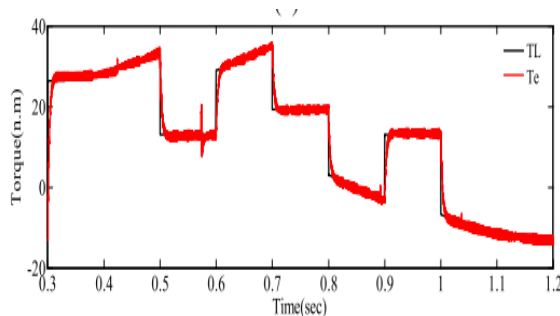
https://doi.org/10.5281/zenodo.14090580

Tracking torque and speed have been observed in order to demonstrate the proper operation of the DTC in BLDC motor. On the basis of the measured standard cycle and load torque, Fig. 10 depicts the speed and torque control of the traditional DTC. As can be seen, the proposed approach performs well as seen by its quick dynamic response and low torque ripple. The output signals follow the intended reference signals, as well. The SOC of the systems, which will be detailed in the following sections, is the primary distinction between the standard DTC and the proposed modified DTC.
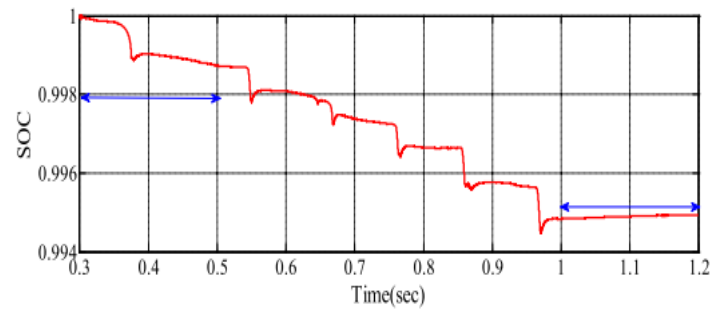
6.2. Modified DTC

The speed and torque signals as determined by assessing the improved DTC method are shown in Fig. 11(a) and (b). A condition that can be used to recover kinetic energy and charge the batteries is the driving cycle with braking and negative acceleration.
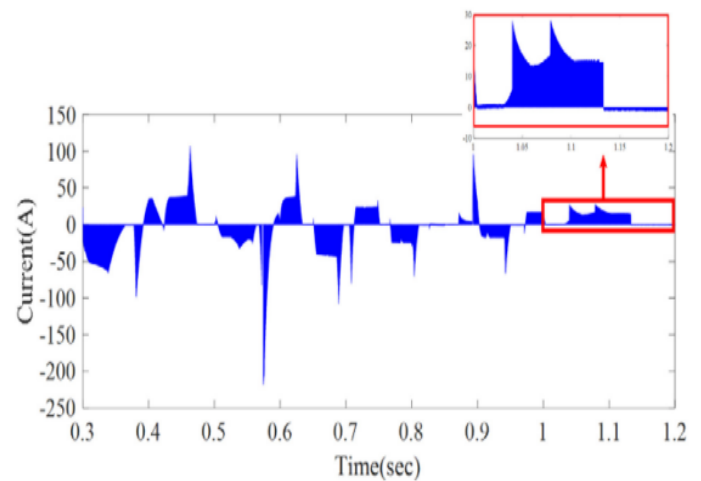
©

(d)

Fig. 11. (a) Speed tracking and references speed, (b) actual Torque tacking with desired torque, (c) SOC in regeneration mode of DTC, (d) current of switch S1 in the braking mode.
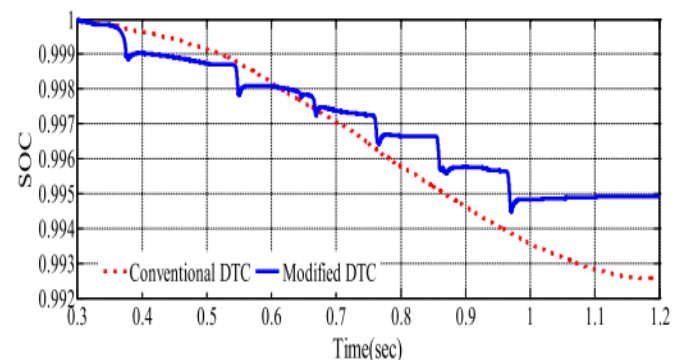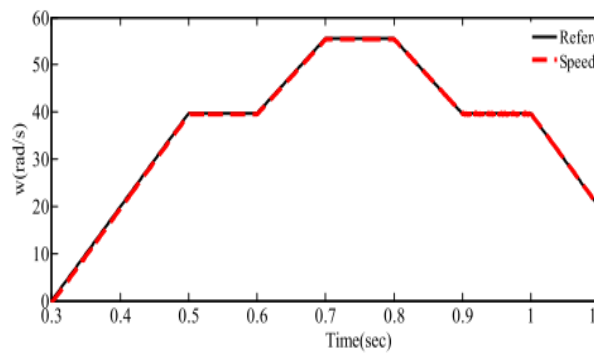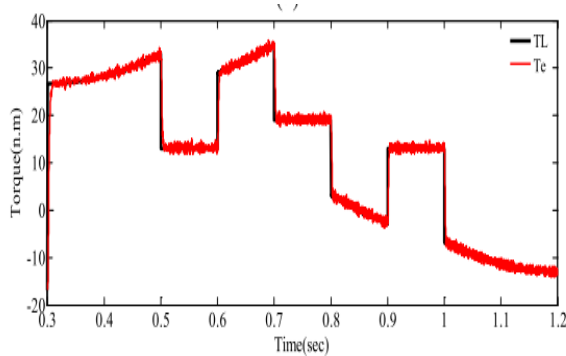
(a)

(b)

Fig. 12. SOC for battery with and without regenerative braking.

It depicts how current travels through the battery pack's battery pack and the inverted diodes D1 and D4.
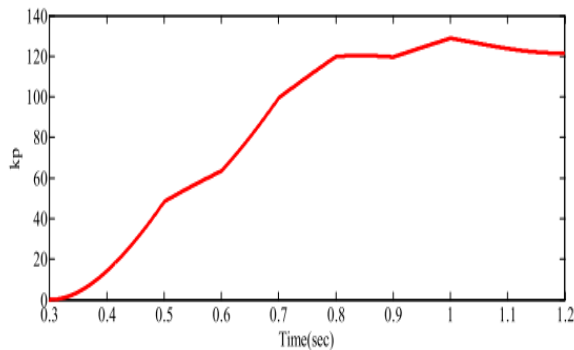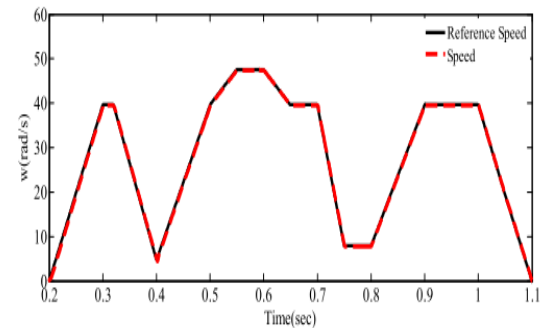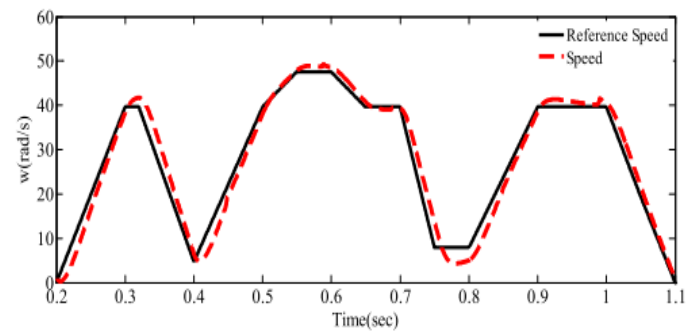

(a)

(b)

©

Fig. 13. (a) Speed tracking, (b) Torque, (c) Adaptive Controller parameter.

Fig. 11(c) depicts the battery's SOC while the vehicle is in regenerative braking mode. As can be observed from the outcome, the battery's SOC has increased. A braking mode is defined as having a considerable speed variation for the time period of 1-1.2 s. The average value of the current is positive in the braking mode, as illustrated in Fig. 11(d), increasing the battery's SOC.
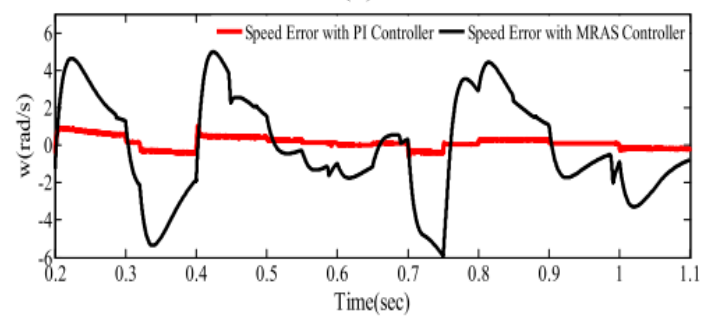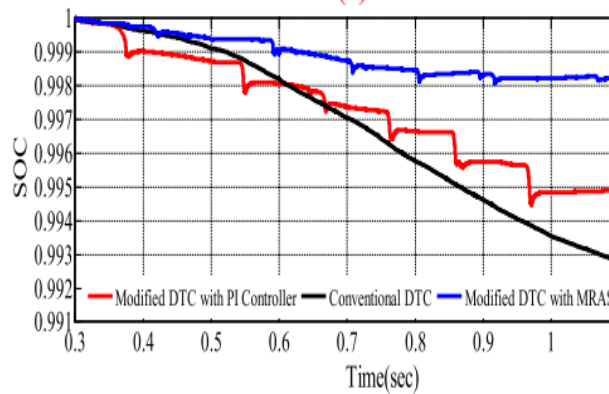

(a)

(b)

©

318

(d)

Fig. 14. (a) Speed tracking of MRAS, (b) speed tracking of PI, (c) speed tracking error for both PI and MRAS controller, (d) SOCs.

6.3. SOC of the DTC and the modified DTC

Figure 12 compares the SOC of the modified DTC and the regular DTC in this circumstance. As can be observed, under the same conditions, the improved DTC method recharged the batteries and restored power at the end of the cycle. However, the SOC has dropped towards the end of the cycle in the traditional DTC approach. When the acceleration is negative, the modified DTC is used to transform the kinetic energy into electric energy.

6.4. MRAS controller

In the final scenario, an adaptive controller has been created to regulate the system and enhance its functionality. When using an adaptive controller, the system will be able to track reference signals well and can help to reduce torque ripples, as depicted in Fig. 13. DTC compares the outcomes of the modified DTC and the traditional DTC. Whereas the improved DTC eliminates the torque and speed ripples, approach has lower tracking error. The adaptive controller is a suitable choice to satisfy the system's performance without

changing the parameters because it has a straightforward and trustworthy method. Based on the simulated findings, the torque ripple is far less than with a PI controller, in addition to the speed and torque being tracked accurately.

Another crucial aspect to demonstrate its effectiveness is adaptability, thus a fresh reference signal is used to track the speed. The suggested adaptive controller has a satisfactory performance without any modifications to the parameters, as demonstrated in Fig. 14, whereas the PI controller cannot follow the new reference signal. The tracking error and torque ripple for both the PI controller and the adaptive controller are shown in Fig. 14(c), where the adaptive controller significantly reduces the tracking error and torque ripple. Additionally, comparing the SOCs demonstrates unequivocally that this condition has the lowest battery energy use.

7. Conclusion

Regenerative braking techniques extend the range of electric cars while minimising maintenance costs. To recover electrical energy from the kinetic energy and return it to the batteries in the motors, a modified direct torque control is proposed. The acceleration during a driving cycle might be positive, negative, or zero. Variations in the load torque are caused by these fluctuations. The simulations are therefore more accurate because of this. The system has a new switching pattern installed as part of the suggested method in order to create electrical energy without making any mechanical adjustments. The simulation findings demonstrate that the revised switching pattern enhances the torque ripples and speed and torque tracking signals. The performance of the suggested algorithm and an improvement in the

amount of energy returned to the batteries are demonstrated by comparing the state of charge patterns of conventional and modified direct torque control. An adaptive controller is created to decrease tracking inaccuracy and torque ripples. The outcomes demonstrate the developed controller's successful operation with various speed reference signals. Results show that both the switched technique used and the model reference adaptive controller are successful in preserving battery life and obtaining the necessary speed tracking. First, comparing the battery's level of charge for the enhanced direct torque control to the standard one reveals a 0.6% improvement over 0.9 s of simulation time. It goes without saying that this quantity of energy can somewhat offset the energy needed for electric vehicles in the actual world. Second, in addition to exhibiting a quicker reaction than a proportional/integral controller and a remarkable reduced error tracking, the model reference adaptive controller has the advantage of simplicity. For a new reference speed, this inaccuracy for the proportional/integral controller ranges between 5.93 and 4.97 rad/s, whereas these values are between 0.63 and 1.04 rad/s for the adaptive controller.

References

[1] Da Xie, Hoaxing Chu, Chenghong Gu, Furlong Li, Zhang Yu. A novel dispatching control strategy for EVs intelligent integrated stations. IEEE Trans Smart Grid 2015;8(2):1–10.

[2] Mohan V, Singh JG, Nogaku W. Sortino ratio-based portfolio optimization considering EVs and renewable energy in microgrid power market. IEEE Trans Sustainable Energy 2017;8(1):219–29.

[3] Chi-land C, Xiao-gang W, Yue-wee B, Yan-chum X, Kai L. Motor drive system design for electric vehicle. IEEE international electric information and control engineering conf. 2011. p. 15–7.

[4] Long B, Lim ST, Ryu JH, Chong KT. Energy-regenerative braking control of electric vehicles using three-phase brushless direct-current motors. Energies 2014; 7:99–114.

[5] Thakor N, Farah E, Ghanbari T. A bi-directional battery charger with modular integrated charge equalization circuit. IEEE Trans Power Electronics 2017;32(3):2133–45.

[6] Mohammad A, ZiaurRahmanKhan MD. BLDC motor controller for regenerative braking. International conference on electrical engineering and information & communication technology (ICEEICT). 2015. p. 1–6.

[7] Nia pour SKM, Garjan GS, Shafiei M, Feyzi MR, Danyal S, &Koushik MB. Review of Permanent-magnet brushless DC motor basic drives based on analysis and simulation study. Int Rev Electra Eng (IREE) 2014;9(5):930–57.

[8] Acaricide SM, Amini M. Design and comparison of axial-flux pm bldc motors for direct drive electric vehicles: conventional or similar slot and pole combination. Int J Eng Innovations Res 2017;6(1).

[9] Shirvani Broaden M, et al. Torque ripple reduction of brushless DC motor based on adaptive input-output feedback linearization. ISA Trans 2017. http://dx.doi.org/10.1016/j.isatra.2017.05.006i.

[10] Nian X, Peng F, Zhang H. Regenerative braking system of electric vehicle driven by brushless DC motor.

IEEE Trans Ind Electron 2014;61(10):5798–808.

[11] Sajitha P, Jasper A. Direct torque control of a BLDC motor based on computing technique. IOSR J Electra Electron Eng 2013;6(6):01–8.

[12] Karthikeyan J, Sekaran RD. Current control of brushless DC motor based on a common DC signal for space operated vehicles. Electric Power Energy Sits 2011; 33:1721–7.

[13] Sadat AR, Pashaei A, Tohidi S, Sharifian MBB. A novel SVM-DTC method of in- wheel switched reluctance motor considering regenerative braking capability in electric vehicle. Int J Tech Phys Prob Eng (IJTPE) 2016;8(4):19–25.

[14] Qiu CN, Wanga G. New evaluation methodology of regenerative braking contribution to energy efficiency improvement of electric vehicles. Energy Convers Manage 2016; 119:389–98.

[15] Khashayar Asadi, Hariharan Ram Shankar, Harish Pellagra, Aishwarya Bhandari, Suraj Shanbhag, Pooja Mehta, Spontoon Kundu, Kevin Han, Edgar Lobaton, Tianfu Wu Building an integrated mobile robotic system for real-time applications in construction, arXiv:1803.01745, 2018.

[16] Zaky MS, Metal MK. A performance investigation of a four-switch three-phase inverter-fed IM drives at low speeds using fuzzy logic and PI controllers. IEEE Trans Power Electron 2016;32(5):3741–53.

[17] Shigeo Zhao, Dan Lei, Jiayi Chen, Hangyu Li. Optimal control of mode transition for four-wheel-drive hybrid electric vehicle with dry dual-clutch transmission. Mech Syst Signal Process 2018;105(May (15)):68–89.

[18] Mao K, Liu G. An improved braking control method for the magnetically levitated TMP with a fast transient response. Vacuum 2018. doi: 10.1016/j.vacuum.2017.12.002.

[19] Kyle S, Hasid A, Kurnia MR. Electric vehicle conversion based on distance, speed, and cost requirements. 2nd international conference sustainable energy engineering and application, energy proedria. 68. 2015. p. 446–54.

[20] Han W, Lee TY, Kim YJ, Jung SY. Comparative analysis on efficiency of brushless DC motor considering harmonic component of phase current and iron loss. 18th international conf on electrical machines and system (ICEMS). 2015.

[21] Parrikar N, Shafiei M, Koushik MB. Direct torque control of brushless DC motor drives with reduced starting current using fuzzy logic controller. Uncertainty reasoning and knowledge engineering (URKE), 2011 international conference on. 1. IEEE; 2011. p. 129–32.

[22] Sharifian MBB, Shafiei M, Sadeghi MS, Goldstone F. Direct torque control of brushless DC motor drives based on ANFIS controller with fuzzy supervisory learning. Electrical machines and systems (ICEMS), 2011 international conference on. IEEE; 2011. p. 1–6.

[23] Gere S, Shafiei M, Saami AR, Alavi S. Position sensor less and adaptive speed design for controlling brushless DC motor drives. Power symposium (NAPS), 2017. IEEE; 2017. p. 1–6.

[24] Bagherpour HM, Salamis FR. 'Robust model reference adaptive output feedback tracking for uncertain linear systems with actuator fault based on reinforced dead-zone modification'. ISA Trans 2015; 57:51–6.

[25] Rehman WU, Wang S, Wang X, Shi C, Zhang C, Tanovic M. Adaptive control for motion synchronization of HA/EHA system by using modified MIT Rule. 11th IEEE conference industrial electronics and applications. 2016.